Improvement of Spin Transfer Torque in Asymmetric Graphene Devices

Chia-Ching Lin, Yunfei Gao, Ashish Verma Penumatcha, Vinh Quang Diep, Joerg Appenzeller, and Zhihong Chen*

School of Electrical and Computer Engineering and Birck Nanotechnology Center, Purdue University, West Lafayette, Indiana, United States

ABSTRACT A graphene lateral spin valve structure with asymmetric contacts is presented for the first time, with enhancement of spin angular momentum absorption in its receiving magnet. The asymmetric device with tunneling barrier only at the injector magnet shows a comparable spin valve signal but lower electrical noises compared to the device with two tunneling barriers. We also report experimental measurements of spin transfer torque. Assisted by an external magnetic field of 2.5 mT, spin diffusion current-induced magnetization reversal occurs at a nonlocal charge current density of 33 mA/μm^2, smaller than that needed in devices with two tunneling barriers.

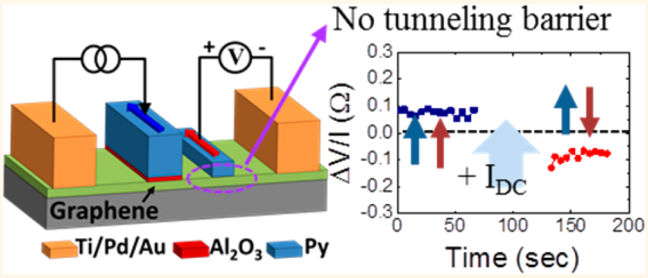

KEYWORDS: graphene · asymmetric contact · tunneling barrier · nonlocal spin valve · spin transfer torque · all-spin logic

Graphene has been experimentally identified as an ideal channel material for spin conduction.[1,2] Spin transport over 20 μm and spin diffusion lengths up to 5 μm have been observed at room temperature.[3,4] However, to further develop a graphene-based spin logic,[5] spin transfer torque[6,7] needs to be demonstrated in graphene devices to show that spin information can be communicated to the outputs. Several groups have theoretically investigated both the spin transport and spin transfer torque behaviors in graphene with various device structures by employing the nonequilibrium Green function method.[8−10] Recently, spin transfer torque has been experimentally demonstrated in lateral nonlocal graphene spin valve devices.[11] Assisted by an external magnetic field, magnetization reversal of the ferromagnetic receiving magnet is induced by pure spin diffusion currents from the injector magnet. While scaling down the size of the ferromagnetic receiving magnet is necessary to reduce the critical spin current needed for spin transfer torque, and ultimately is needed to eliminate the external field assistance, it is also imperative to improve the spin angular momentum absorption at the interface between graphene and the receiving magnet.

To achieve sufficient spin injection from ferromagnetic contacts into the graphene channels in conventional graphene lateral nonlocal spin valve devices, tunneling barriers are normally inserted at both injector and detector contacts to reduce the conductance mismatch between the magnets and graphene channels and contact-induced spin relaxation as well.[2,12−15] This device structure is also adopted in our first graphene spin torque device.[11] However, the barrier underneath the receiving magnet limits spin angular momentum transfer due to its high resistance, which poses an additional challenge in graphene-based spin transfer torque devices. In this article, we report a new graphene spin device design with the tunneling barrier at the receiving magnet being removed, which leads to a high spin absorption. The measured nonlocal spin valve signal has lower noise, and its magnitude is comparable to a conventional device with two barriers. More importantly, the critical spin torque current density is greatly reduced.

RESULTS AND DISCUSSION

To directly compare the nonlocal spin valve signals (R_S) of the devices with single and double tunneling barriers, two lateral spin valve devices with five electrodes are fabricated on the same peeled graphene flake, as shown in Figure 1. The graphene flake thickness is identified to be six layers

* Address correspondence to zhchen@purdue.edu.

Received for review January 27, 2014 and accepted March 17, 2014.

Published online March 17, 2014
10.1021/nn500533b

by optical contrast and atomic force microscope (AFM). Under electrode 3, a thin Al_2O_3 film oxidized from 0.6 nm deposited Al serves as a tunneling barrier prior to the deposition of 25 nm permalloy (Py). The same structure is used for electrode 2, while no tunneling barrier is inserted under electrode 4. Nonmagnetic Ti/Pd/Au contacts are used for electrodes 1 and 5 for analysis simplicity and provide low contact resistances in charge transport. In our unique setup, the two spin valve devices share the same graphene flake and a common injector (electrode 3) and have detectors with (electrode 2) or without (electrode 4) a tunneling barrier. Unambiguously, the function of the Al_2O_3 tunneling barrier at the detector can be quantitatively studied. All measurements are performed at 77 K using standard ac lock-in technique. A gate voltage (V_G) of +40 V is applied to the Si substrate to enable a large spin diffusion length that can be achieved at high carrier concentrations.[4,16−18]

The measurement setup for the two devices is illustrated in Figure 2a, and the nonlocal spin valve resistance, $\Delta V/I$, is plotted in Figure 2b as a function of the external magnetic field along the easy axis of the Py magnets. The measured R_S (~0.2 Ω), the resistance difference between the parallel (P) and antiparallel (AP) state, is very similar for both devices. However, electrical noises greatly decrease from 8.4% in the double-barrier device to 4.5% in the single-barrier device. The reduction of the electrical noises is consistently observed in all single-barrier devices, which indicates that removing one tunneling barrier eliminates a critical noise source. It is likely that the oxidized Al film contains defects and trapped charges that can induce additional electrical noises.[19] To further understand why similar signals are measured from the two devices, we evaluate R_S by the general spin accumulation signal equation. Because the spin resistance of the graphene channel is much larger than that of the Py magnet and the interfacial current polarization is rather small in graphene spin devices, we can modify the general R_S equation[20] as follows:

$$R_S = 4R_N P_{C,\text{injector}} P_{C,\text{detector}} \times \frac{\left(\frac{R_{C,\text{injector}}}{R_N}\right)\left(\frac{R_{C,\text{detector}}}{R_N}\right)\exp\left(-\frac{L}{\lambda_S}\right)}{\left(1+\frac{2R_{C,\text{injector}}}{R_N}\right)\left(1+\frac{2R_{C,\text{detector}}}{R_N}\right)-\exp\left(-\frac{2L}{\lambda_S}\right)} \quad (1)$$

where $R_N = \rho_\square \lambda_S / W$, is the graphene spin resistance, with λ_S being the spin diffusion length of graphene and $\rho_\square$ being the graphene sheet resistivity, P_C is the interfacial current polarization, R_C is the contact resistance, L is the channel length, and W is the channel width. In the presented multilayer graphene device, $L = 0.4\ \mu$m and $W = 1.0\ \mu$m. From four-probe measurements, we find $\rho_\square = 0.8$ kΩ, $R_C = 2$ kΩ with tunneling barrier, and $R_C = 1$ kΩ without tunneling barrier. From our previous work on devices with various channel lengths we extracted $\lambda_S = 4.2 \pm 0.5\ \mu$m and $P_C = 4 \pm 1\%$.[4] The ratio of the resistance values, $R_{S,\text{Single}}$ (one barrier) and $R_{S,\text{Double}}$ (two barriers), calculated from eq 1 falls into the range 0.45 < ratio <1.25 with an average value of 0.75, in agreement with our experimental observation of a negligible difference between the measured signals for the one- and two-barrier case.

Thus far, the device without a tunneling barrier in the detector is found to deliver comparable spin valve signals with lower noise and lower contact resistance at the detector interface if compared to the conventional structure with double tunneling barriers. These are all key factors for efficient spin transfer torque.

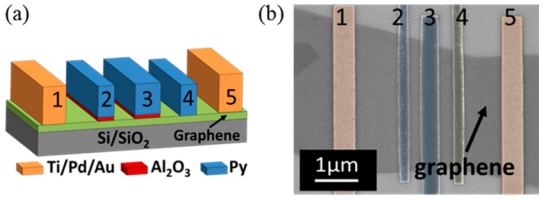

Figure 1. Graphene lateral spin valve device with five electrodes. (a) Schematic and (b) SEM of the device. The dimensions of the Py injector (electrode 3) is 400 nm (W) × 25 nm (H) with a tunneling barrier formed from an oxided Al film (0.6 nm). The dimensions of the Py detectors (electrodes 2 and 4) are 200 nm (W) × 25 nm (H). Only electrode 2 possesses a tunneling barrier underneath, while electrode 4 does not. The spaces between the injector and the two detectors are both 400 nm.

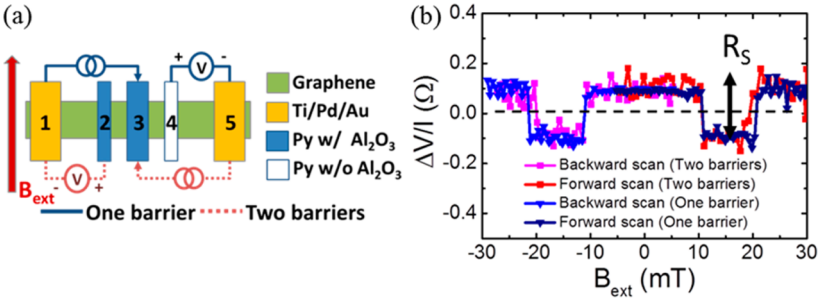

Figure 2. (a) Measurement configurations of the two graphene lateral spin valve devices with single and double tunneling barriers. The charge current is injected from electrode 3. The voltage is measured between electrodes 1 and 2 for the double tunneling barrier device and between electrodes 4 and 5 for the single tunneling barrier device. (b) Nonlocal spin valve signal ($\Delta V/I$) measured at $V_G = +40$ V for the two devices.

Next we demonstrate a magnetization reversal by spin transfer torque in the presence of an external magnetic field, in a seven-layer graphene device with the asymmetric tunneling barrier structure as described above. The thickness of the Py detector magnet is scaled down to 5 nm (see Figure 3a), allowing for magnetization switching.[21,22] The nonlocal spin valve measurements as a function of the external magnetic field along the easy axis of the Py magnets are presented in Figure 3b. Note that the coercive field strongly decreases with the thickness of the magnet.[11] The two transitions in Figure 3b correspond to the switching of the 5 nm detector at ±3.5 mT and the 25 nm injector at ±22 mT. Knowing the coercive field of the two magnets, we preset the two magnets to a parallel state aligned to the negative magnetic field direction. The external field is then scanned from negative to positive and stopped at +2.5 mT, which is smaller than the coercive field (+3.5 mT) of the detector. A positive current pulse of +4 mA is injected for a duration of 5 μs from the injector magnet. Note that the positive current extracts the spins that are preset to be aligned to the negative field direction from the graphene channel, leaving spins aligned to the positive field accumulated underneath the injector. These "opposite spins" propagate through the graphene channel, arrive at the detector, and switch its magnetization to the positive field direction. Now the preset P state changes to the AP state as shown in Figure 4a. Next, we continue to scan the external magnetic field from +2.5 mT to +30 mT. As shown in Figure 4b, no sharp change of $\Delta V/I$ is observed at +3.5 mT, which is the coercive field of the detector, a clear evidence that the magnetization of the detector has already been switched by the spin current.

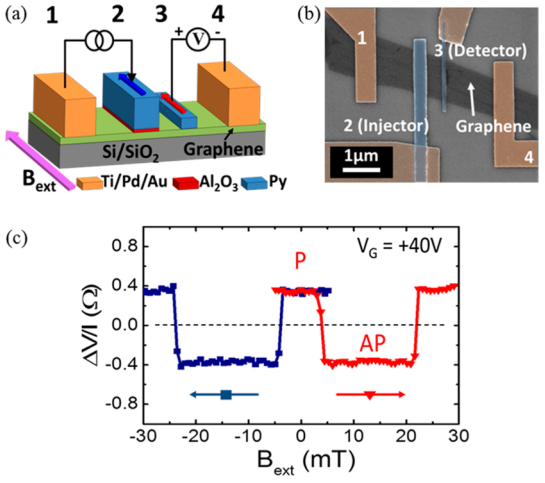

Figure 3. Graphene spin valve device with asymmetric contacts. (a) Schematic and SEM of the device. The dimensions of the Py injector are 300 nm (W) × 25 nm (H) with an Al_2O_3 tunneling barrier. The Py detector is 100 nm (W) × 5 nm (H). The space between two Py magnets is 300 nm, and the channel width is 1.2 μm. (b) Nonlocal spin valve signal ($\Delta V/I$) measured at V_G = +40 V. The sharp changes in $\Delta V/I$ at ±3.5 and ±22 mT are related to the coercive fields of the two Py magnets.

The critical charge current for the spin transfer torque in this presented asymmetric device structure with a tunneling barrier only at the injector side is 4 mA with the assistance from a magnetic field of +2.5 mT. The difference between the coercive field (+3.5 mT) of the detector and the assistant magnetic field, ΔB = 1 mT, is exactly the same preset condition as in our previous report,[11] where spin transfer torque of a graphene device with double tunneling barriers was observed. We have also ensured that the two device structures have the same layout and the same graphene layer number and quality, which allows us to compare the spin transfer torque efficiency in these two structures with the only difference being the tunnel barrier at the detector side. To compare the switching efficiency of these two devices, the critical charge current is normalized by the contact area of the detector. The critical charge current density needed for spin transfer torque in the single tunneling barrier device presented in this article is calculated to be 33 mA/μm^2, while that for the double tunneling

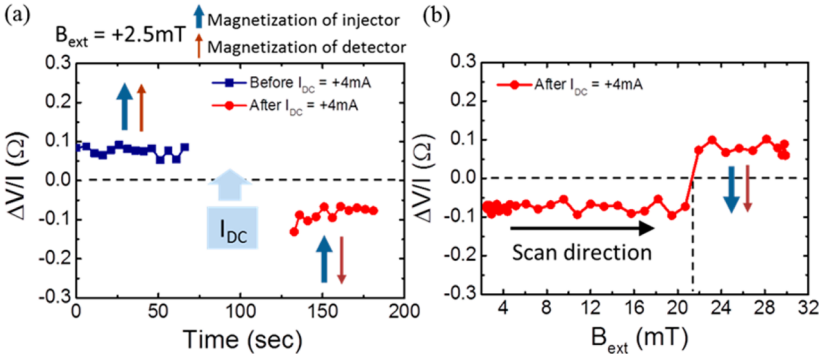

Figure 4. Spin transfer torque measurements. (a) Nonlocal spin valve measurement as a function of time during the spin torque experiment. A clear $\Delta V/I$ change is seen before and after a dc current pulse of +4 mA is applied, indicating a P to AP switching. (b) Nonlocal spin valve measurement scan after a dc current pulse of +4 mA. No $\Delta V/I$ transition is observed at 3.5 mT since the detector is already switched. $\Delta V/I$ changes at +22 mT, at which the injector is switched by the external magnetic field.

barrier device presented in ref 11 is calculated to be 45 mA/μm^2; a substantial reduction is obtained by our asymmetric device design.

To theoretically understand the above improvement, we use the spin circuit model[23] to estimate the critical charge current ($I_{C,\ \mathrm{critical}}$) for the two structures. In the spin circuit model, the individual components of the nonlocal spin valve structure (the magnets, the interfaces, and the graphene channel) can be analyzed independently. Once the charge current, I_C, is injected into the device, we can calculate the spin voltage and spin current in each component. The spin voltage underneath the detector magnet is defined as $V_{S,D}$. On the basis of the ref 20, G_{tot} is the spin conductance of the detector, which includes conductance contributions from both the magnet (G_F) and the contact interface ($G_{C,\ \mathrm{detector}}$). Note that, even in the detector without a tunneling barrier layer, there is a barrier at the interface because the metal-induced doping of graphene leads to a Fermi energy difference between the graphene under the contact and in the channel area.[24,25] Different from conventional Schottky contacts at metal/semiconductor interfaces,[26,27] the magnitude of this barrier can be modulated by the Si back gate. But even in the device on-state at $V_G = +40$ V, a contact resistance of >200 Ω-μm is often measured.[24] Hence, for graphene devices, $G_F \gg G_{C,\ \mathrm{detector}}$, and $G_{tot} \approx G_{C,\ \mathrm{detector}}$. The spin current polarization of the detector, P_{tot}, also has contributions from both the magnet (P_F) and the interface ($P_{C,\ \mathrm{detector}}$). Again, due to the large G_F value, $P_{tot} = (G_F P_{C,\mathrm{detector}} + G_{C,\mathrm{detector}} P_F)/(G_F + G_{C,\mathrm{detector}}) \approx P_{C,\mathrm{detector}}$. The spin current flowing into the detector (I_S) can be calculated as $I_S = V_{S,D} G_{tot}$. On the other hand, the nonlocal spin valve signal (R_S) we measured at I_C can be calculated as $R_S = (V_{S,D} P_{tot})/I_C$. Therefore, the spin current, I_S, in the graphene case can be written as

$$I_S = \frac{I_C R_S}{P_{tot}} G_{tot} \approx \frac{I_C R_S}{P_{C,\ \mathrm{detector}}} G_{C,\ \mathrm{detector}} = \frac{I_C R_S}{P_{C,\ \mathrm{detector}} R_{C,\ \mathrm{detector}}} \quad (2)$$

Let us define the critical charge current for spin torque as $I_{C,\mathrm{critical}}$, and the critical spin current as $I_{S,\mathrm{critical}}$. Given the same contact area and thickness of the detector magnet in devices with and without a tunnel barrier, the critical spin current, $I_{S,\mathrm{critical}}$, is the same for both device structures. Therefore, the ratio of $I_{C,\mathrm{critical}}$ of the two device structures can be expressed as follows:

$$\frac{I_{C,\ \mathrm{single}}}{I_{C,\ \mathrm{double}}} = \frac{R_{S,\ \mathrm{double}}}{R_{S,\ \mathrm{single}}} \frac{R_{C,\ \mathrm{w/o\ barrier}}}{R_{C,\ \mathrm{w/\ barrier}}} \frac{P_{C,\ \mathrm{w/o\ barrier}}}{P_{C,\ \mathrm{w/\ barrier}}} \quad (3)$$

On the basis of our spin valve signal analysis for eq 1 above, $R_{S,\mathrm{single}}/R_{S,\mathrm{double}} = 0.75$, together with $R_{C,\mathrm{w/o\ barrier}} \approx 1$ kΩ, $R_{C,\mathrm{w/\ barrier}} \approx 2$kΩ, and $P_{C,\mathrm{w/o\ barrier}} \approx P_{C,\mathrm{w/\ barrier}}$, we estimate the critical charge current ratio to be 0.67, which is very close to our experimental observation of ratio ~33/45 = 0.73.

To further understand the spin transfer torque mechanism in our graphene devices, we first calculate the spin current flowing into the detector (I_S) based on eq 2 above. Given the parameters in our presented device—$I_C = 4.0$ mA, $R_S = 0.8$ Ω, $P_{C,\mathrm{detector}} \approx 4\%$, and $R_{C,\mathrm{detector}} \approx 1$ kΩ—I_S can be approximated as ~80 μA. On the other hand, the critical spin current for spin transfer torque through the Slonczewski (anti-damping spin torque) mechanism[6,7] alone is calculated using Sun's macrospin model.[28] The critical spin current is derived as $(\alpha e M_S V_{vol} \mu_0)/\hbar$, where α is the Gilbert damping constant, M_S is the Py magnetization, V_{vol} is the volume of the Py detector, and μ_0 is the permeability in a vacuum. It is approximated to be ~3 mA for the volume of the Py detector in our device. On the basis of these two simple calculations, we do not expect spin transfer torque through the Slonczewski mechanism alone in our device due to the very large easy-plane anisotropy. This is also why an external magnetic field along the easy axis is needed to assist the spin transfer torque. As discussed in our previous publication,[11] we suggest the contribution from a field-like spin torque effect[29−31] is significant in our experimental demonstration. Most importantly, the field-like term is treated as an effective field. With an external magnetic field assist, the critical spin current of spin transfer torque through the field-like term is significantly reduced.[11]

Other potential mechanisms for magnetization reversal have been ruled out by a number of control experiments and theoretical estimation. Details of the control experiments can be found in the Supporting Information of ref 11. To summarize our findings, in the same device, (1) under the same preset conditions, negative current pulses cannot result in the P to AP switching, excluding current-induced heating being responsible for the switching; (2) when aligning the two magnets in positive magnetic fields, with assistance of negative magnetic fields no spin transfer torque is observed at negative current pulses. Note that, in the current-induced Oersted field switching, a preset P state aligned to the negative magnetic field needs a positive current to switch to an AP state, and a P state aligned to the positive field needs a negative current to switch, which is not what we observe in our spin transfer torque measurements, therefore ruling out the possibility of the current-induced Oersted field switching. The impact of thermal activation on spin transfer torque[32] in our nonlocal device geometry with a current pulse injected at 77 K for 5 μs is calculated to play a negligible role. We have adopted the strict model used for current-perpendicular local spin-valve type devices[33] to estimate the maximum thermal activation effect to be ~13% of the intrinsic critical charge current density. Note that over the 300 nm

distance between the two magnets in our nonlocal device structure, the thermal activation impact on the detector side will further decay.

CONCLUSION

In conclusion, spin valve signals are measured in nonlocal graphene lateral spin devices with tunneling barriers only at the injector magnets. The electrical noise is 2 times lower if compared to that of the conventional double tunneling barrier structures. The experimental demonstration of spin transfer torque assisted by an external magnetic field is also presented in this asymmetric device structure for the first time. The critical charge current density is reduced due to the improvement of spin absorption at the detector.

METHODS

Graphene flakes were mechanically exfoliated from highly oriented pyrolytic graphite onto heavily doped silicone substrates with 90 nm silicon dioxide on top. Graphene layer number was identified by optical contrast and atomic force microscope. Metal electrodes were defined by electron beam lithography, followed by a metalization and lift-off process. For the ferromagnetic electrodes containing a tunneling barrier, a thin film of oxidized Al (0.6 nm) was inserted between the permalloy and the graphene channel. A stack of Ti/Pd/Au (1 nm/20 nm/20 nm) metal layers was used for nonmagnetic electrodes. All nonlocal spin valve measurements were performed at 77 K using the standard ac lock-in technique. A gate voltage of +40 V was applied to the Si substrate during measurements. For the spin torque demonstration experiment, a direct current (dc) pulse with a duration of 5 μs was injected into the injector magnet, while the magnetization of the detector was monitored through nonlocal spin valve measurements.

Conflict of Interest: The authors declare no competing financial interest.

Acknowledgment. We would like to acknowledge our very fruitful conversations with Prof. Supriyo Datta. We also gratefully acknowledge the support of this work by Nanoelectronics Research Initiative (NRI) through the Institute for Nanolectronics Discovery and Exploration (INDEX) Center.

REFERENCES AND NOTES

1. Hill, E. W.; Geim, A. K.; Novoselov, K.; Schedin, F.; Blake, P. Graphene Spin Valve Devices. *IEEE Trans. Magn.* **2006**, *42*, 2694–2696.
2. Tombros, N.; Jozsa, C.; Popinciuc, M.; Jonkman, H. T.; van Wees, B. J. Electronic Spin Transport and Spin Precession in Single Grapheme Layers at Room Temperature. *Nature* **2007**, *448*, 571–574.
3. Zomer, P. J.; Guimaraes, M. H. D.; Tombros, N.; van Wees, B. J. Long-Distance Spin Transport in High-Mobility Graphene on Hexagonal Boron Nitride. *Phys. Rev. B* **2012**, *86*, 161416.
4. Gao, Y.; Kubo, Y.; Lin, C. C.; Chen, Z.; Appenzeller, J. Optimized Spin Relaxation Length in Few Layer Graphene at Room Temperature. *IEEE Electron Devices Meeting (IEDM) 2012*; San Francisco, December 10 to 13, 2012; 10.1109/IEDM.2012.6478978.
5. Behin-Aein, B.; Datta, D.; Salahuddin, S.; Datta, S. Proposal for an All-Spin-Logic Device with Built-In Memory. *Nat. Nanotechnol.* **2010**, *5*, 266–270.
6. Slonczewski, J. C. Current-Driven Excitation of Magnetic Multilayers. *J. Magn. Magn. Mater.* **1996**, *159*, L1–L7.
7. Berger, L. Emission of Spin Waves by a Magnetic Multilayer Traversed by a Current. *Phys. Rev. B* **1996**, *54*, 9353–9358.
8. Zhou, B.; Chen, X.; Wang, H.; Ding, K. H.; Zhou, G. Magnetotransport and Current-Induced Spin Transfer Torque in a Ferromagnetically Contacted Graphene. *J. Phys.: Condens. Matter* **2010**, *22*, 445302.
9. Zhou, B.; Chen, X.; Zhou, B.; Ding, K. H.; Zhou, G. Spin-Dependent Transport for Armchair-Edge Graphene Nanoribbons between Ferromagnetic Leads. *J. Phys.: Condens. Matter* **2011**, *23*, 135304.
10. Krompiewski, S. Effect of the Attachment of Ferromagnetic Contacts on the Conductivity and Giant Magnetoresistance of Graphene Nanoribbons. *Nanotechnology* **2012**, *23*, 135203.
11. Lin, C. C.; Penumatcha, A. V.; Gao, Y.; Diep, V. Q.; Appenzeller, J.; Chen, Z. Spin Transfer Torque in a Graphene Lateral Spin Valve Assisted by an External Magnetic Field. *Nano Lett.* **2013**, *13*, 5177–5181.
12. Schmidt, G.; Ferrand, D.; Molenkamp, L. W. Fundamental Obstacle for Electrical Spin Injection from a Ferromagnetic Metal into a Diffusive Semiconductor. *Phys. Rev. B* **2000**, *62*, R4790–R4793.
13. Rashba, E. I. Theory of Electrical Spin Injection: Tunnel Contacts as a Solution of The Conductivity Mismatch Problem. *Phys. Rev. B* **2000**, *62*, R16267–R16270.
14. Fert, A.; Jaffrès, H. Conditions for Efficient Spin Injection from a Ferromagnetic Metal into a Semiconductor. *Phys. Rev. B* **2001**, *64*, 184420.
15. Han, W.; Pi, K.; McCreary, K. M.; Li, Y.; Wong, J. J. I.; Swartz, A. G.; Kawakami, R. K. Tunneling Spin Injection into Single Layer Graphene. *Phys. Rev. Lett.* **2010**, *105*, 167202.
16. Goto, H.; Kanda, A.; Sato, T.; Tanaka, S.; Ootuka, Y.; Miyazaki, H.; Tsukagoshi, K.; Aoyagi, Y. Gate Control of Spin Transport in Multilayer Graphene. *Appl. Phys. Lett.* **2008**, *92*, 212110.
17. Maassen, T.; Dejene, F. K.; Guimaraes, M. H. D.; Jozsa, C.; van Wees, B. J. Comparison between Charge and Spin Transport in Few-Layer Graphene. *Phys. Rev. B* **2011**, *83*, 115410.
18. Jozsa, C.; Maassen, T.; Popinciuc, M.; Zomer, P. J.; Veligura, A.; Jonkman, H. T.; van Wees, B. J. Linear Scaling between Momentum and Spin Scattering in Graphene. *Phys. Rev. B* **2009**, *80*, 241403.
19. Nowak, E. R.; Weissman, M. B.; Parkin, S. S. P. Electrical Noise in Hysteretic Ferromagnet-Insulator-Ferromagnet Tunnel Junctions. *Appl. Phys. Lett.* **1999**, *74*, 600–602.
20. Takahashi, S.; Maekawa, S. Spin Injection and Detection in Magnetic Nanostructures. *Phys. Rev. B* **2003**, *67*, 052409.
21. Zhang, J.; Levy, P. M.; Zhang, S.; Antropov, V. Identification of Transverse Spin Currents in Noncollinear Magnetic Structures. *Phys. Rev. Lett.* **2004**, *93*, 256602.
22. Yang, T.; Kimura, T.; Otani, Y. Giant Spin-Accumulation Signal and Pure Spin-Current-Induced Reversible Magnetization Switching. *Nat. Phys.* **2008**, *4*, 851–854.
23. Srinivasan, S.; Diep, V.; Behin-Aien, B.; Sarkar, A.; Datta, S. Modeling Multi-Magnet Networks Interacting *via* Spin Currents. *arXiv.org* **2013**, arXiv:1304.0742.
24. Knoch, J.; Chen, Z.; Appenzeller, J. Properties of Metal-Graphene Contacts. *IEEE Trans. Nanotechnol.* **2012**, *11*, 513.
25. Farmer, D. B.; Golizadeh-mojarad, R.; Perebeinos, V.; Lin, Y.; Tulevski, G. S.; Tsang, J. C.; Avouris, P. Chemical Doping and Electron−Hole Conduction Asymmetry in Graphene Devices. *Nano Lett.* **2009**, *9*, 388–392.
26. Hanbicki, A. T.; van't Erve, O. M. J.; Magno, R.; Kioseoglou, G.; Li, C. H.; Jonker, B. T.; Itskos, G.; Mallory, R.; Yasar, M.; Petrou, A. Analysis of the Transport Process Providing Spin Injection through an Fe/AlGaAs Schottky Barrier. *Appl. Phys. Lett.* **2003**, *82*, 4092–4094.

27. Chung, N. L.; Jalil, M. B. A.; Tan, S. G. The Effects of Schottky Barrier Profile on Spin Dependent Tunneling in a Ferromagnet-Insulator-Semiconductor System. *J. Appl. Phys.* **2010**, *108*, 034503.
28. Sun, J. Z. Spin-Current Interaction with Monodomain Magnetic Body: A Model Study. *Phys. Rev. B* **2000**, *62*, 570–578.
29. Zhang, S.; Levy, P. M.; Fert, A. Mechanisms of Spin-Polarized Current-Driven Magnetization Switching. *Phys. Rev. Lett.* **2002**, *88*, 236601.
30. Ralph, D. C.; Stiles, M. D. Spin Transfer Torques. *J. Magn. Magn. Mater.* **2008**, *320*, 1190–1216.
31. Brataas, A.; Kent, A. D.; Ohno, H. Current-Induced Torques in Magnetic Materials. *Nat. Mater.* **2012**, *11*, 372–381.
32. Myers, E. B.; Albert, F. J.; Sankey, J. C.; Bonet, E.; Buhrman, R. A.; Ralph, D. C. Thermally Activated Magnetic Reversal Induced by a Spin-Polarized Current. *Phys. Rev. Lett.* **2002**, *89*, 196801.
33. Koch, R. H.; Katine, J. A.; Sun, J. Z. Time-Resolved Reversal of Spin-Transfer Switching in a Nanomagnet. *Phys. Rev. Lett.* **2004**, *92*, 088302.